Thin Solid Films 703 (2020) 137975

Contents lists available at ScienceDirect

Thin Solid Films

journal homepage: www.elsevier.com/locate/tsf

The effect of morphology on the ozone-gas sensing properties of zinc oxide sputtered films

Y.N. Colmenares*, W. Correr, B.S. Lima, V.R. Mastelaro

São Carlos Institute of Physics, University of São Paulo, PO Box 369, São Carlos 13560-970, SP, Brazil

ARTICLE INFO

Keywords:
Metal oxide
Gas sensor
Zinc oxide
Radio-frequency sputtering synthesis
Gas-sensing effects

ABSTRACT

One of the main obstacles in the development and design of semiconductor gas sensors is our limited understanding of the practical mechanisms responsible for sensing. Although theoretical models describe the importance of morphology on the gas sensing properties of semiconductor films, a direct relation between structure size/morphology and gas detection has not been experimentally established. In this work, the Radio-Frequency Sputtering method was used to obtain zinc oxide thin films from ceramic and metallic targets. Remarkable differences in the nanostructure size were observed when distinct powers of deposition were used. The samples were deposited on platinum interdigitated electrodes and exposed to ozone to have their sensing behavior analyzed. The feature size and film porosity were studied taking into consideration the enhancement of sensor performance, while their band gaps showed no significant differences between films. It was found that sensors with small features and low porosity present low ozone sensitivity and fast responses, while highly porous films with large features exhibit low sensitivity and slow responses. The optimum sensing performance was found to be at the apparent maximized surface area, where the best ozone response was observed. Our results show that radio frequency sputtering can be considered a versatile deposition technique for the production of semiconductor gas sensors, since porosity, feature size, and therefore gas sensor sensitivity, can all be controlled through the sputtering parameters of a Zn metallic target followed by thermal oxidation.

1. Introduction

In the past few years, the use of metal oxide semiconductor films as gas-sensing devices has become an important subject in materials science [1]. Because of their exceptional gas-sensing capacity and appealing simplicity, the number of scientific papers addressing semiconductor materials with gas-sensing properties has increased by almost 20% per year since 2011. Besides, their promising properties can potentially solve problems of specificity, detection limits and production of thin-films gas sensors [1–4].

Although the experimental studies of the last few years have registered great improvements in the sensing properties of semiconductors regarding their morphology, crystallinity and dopant presence [5–14], there are still several problems related to selectivity, reproducibility and sensitivity of semiconductor sensors that limit its extended use.

The frontier in this research field stands in the poor understanding of the kinetic molecular mechanism of sensing. According to Barsan et al. [15], the key point for improving and designing thin films for gas sensing is to reduce the enormous gap between the empirical and basic research and use the theoretical approach to produce and use sensing films. As matter of fact, although theoretical models show the dependence of semiconductor sensing response with aspects, such as superficial area, grain interconnection and depletion layer, only a few experimental studies attempt to establish direct relations between those factors and gas sensing. The main reason behind this tendency lies in the experimental limits and complexities of finely controlling the thin-film growth, morphology and composition.

Among the materials used in gas sensor technologies, one of the most important is ZnO. This direct band gap semiconductor (3.37 eV) has been used in a wide range of applications because of its optical, electrical and catalyst properties. The ZnO easy, low-cost synthesis together with the magnitude of the pure material response (comparable with the performance of materials commercially available) make it one of the most researched materials in gas-sensing applications [16]. According to the synthesis method, ZnO assumes a great variety of morphologies–each one with distinct sensing properties according to surface reactivity and electrical properties [16,17]. In the work developed by Alenezi et al. [10], ZnO hierarchical structures exhibit improved gas-sensing performance compared with mono-morphological ZnO and

* Corresponding author.
E-mail address: valmor@ifsc.usp.br (Y.N. Colmenares).

https://doi.org/10.1016/j.tsf.2020.137975
Received 2 July 2019; Received in revised form 4 March 2020; Accepted 22 March 2020
Available online 08 April 2020

commercial ZnO powders. Similar to the behavior of other sensing materials, the greater sensitivity and reduced response speed of these structures are attributable to the high surface-to-volume ratio and formation of secondary junctions of such nanostructured films [9].

In this work, we use the highly-stable growth conditions of the radio frequency (RF) Sputtering method to study the gas-sensing capacities of zinc oxide films in terms of morphology. This technique–not well-explored in gas-sensing development can allows us to control film morphology and, in this sense, modify the surface area available for adsorption, the number of adsorption sites and the conductivity between the grains of ZnO films [18]. Although other authors are demonstrated the influence of the morphology in the gas sensing response of ZnO films [19,20], this work analyze the influence of porosity and structure size (that comes from using different powers of deposition) in the magnitude and times of the response to ozone. In this work the structure size and the apparent area for adsorption (instead of the crystallite or particle size) is directly related to the sensing response of ZnO porous structures.

2. Experimental

2.1. Thin-film deposition

Films were deposited by sputtering a pure metallic zinc or zinc oxide ceramic target into an RF-magnetron sputtering system operating at a radio frequency of 13.5 MHz and powers ranging from 15 to 240 W. The deposition chamber is pumped to a base pressure of 10^{-4} Pa and then filled with argon at a working pressure of 2 Pa. The films were deposited on silica (SiO_2/Si) wafers for characterization. To obtain zinc oxide films from metallic Zn depositions, the samples were oxidized in a furnace at 530 °C with air atmosphere for 12 h.

2.2. Thin-Film Characterization

Grazing-Incidence X-Ray Diffraction (GIXRD) was used to characterize the crystalline structure of the thin films. Since the films are quite thin (< 100 nm), the use of GIXRD reduces substrate contribution. GIXRD patterns were collected in multipurpose Rigaku Ultima IV x-ray diffraction equipment with an incidence angle of 1.5º and a source wavelength of 1.54 Å (Cu-Kα). The patterns were compared with those reported in the crystallographic database ICSD (Inorganic Crystal Structure Database), PDF number #01-079-0205 36-1451, for ZnO (Wurtzite).

To confirm the film composition and discard the presence of contaminants, the films were analyzed by X-ray photoelectron spectroscopy (XPS) in a Scientia Omicron ESCA spectrometer with monochromated x-ray source Al Kα (1486.7 eV). The x-ray source was used with a power of 280 W and a constant pass energy mode of 50 eV. The data analysis was accomplished by *CasaXPS* software (version 2.3.16), and charge effects were corrected using the 1 s carbon peak (284.6 eV) from the adventitious carbon in the surface of the sample.

Scanning Electron Microscopy (SEM) images were obtained using an INSPECT F50 (FEI, The Netherlands) and a Magellan 400 L High-Resolution Microscope (FEI, The Netherlands) operating between 2 and 5 KV. In structure size measurements, circa 200 particles per image were measured using *Image J software*.

To determine the band gap of the films, absorbance spectroscopy was performed using an Agilent Cary 60 UV–Vis spectrophotometer. As a direct band-gap material, the ZnO band gap is computed from the abscissa intersection of the extrapolated straight-line part of the Tauc plot of $(\alpha h\upsilon)^2$ as a function of $h\upsilon$, where α is the absorption coefficient, h is Planck's constant and υ is the light frequency.

2.3. Gas-sensing performance

For the gas-sensing analysis, the ZnO films were deposited on interdigitated (100-nm-thick) platinum electrodes printed in silica (SiO_2/Si) substrates. The interdigitated electrodes were fabricated by sputtering and photolithography techniques in the Microfabrication Laboratory (LMF) at the Brazilian Synchrotron Light Laboratory (LNLS).

The film deposition was performed directly above electrodes and controlled by a quartz crystal microbalance. It is worth mentioning that the same amount of material was deposited each time. All the film thicknesses were confirmed by Atomic Force Microscopy measurements using a FlexAFM (Nanosurf Switzerland).

To perform gas-sensing measurements, the sensors were placed on a heating plate inside a sealed chamber equipped with a gas inlet right above the sensor surface. A constant voltage of 1 V was applied to measure the film electrical resistance by using two needles of gold-coated tungsten on the electrode extremes and a Keithley electrometer. Ozone was produced from dry flowing air illuminated with a pen-ray UV lamp that generated ozone concentrations between 0.05 and 0.89 ppm. The mixture of dry air and ozone was injected right above the sample at a constant flux of 500 ml/min. The baseline was acquired when only dry air was injected. Similarly, to determine the response to hydrogen (H_2), a mixture of hydrogen-nitrogen and dry air was injected in the gas chamber at different volume ratios to control H_2. The sensor response was defined as the ratio between the electrical resistance in the presence of the analyte gas (ozone or hydrogen), R_g, and the resistance under dry air only, R_a.

The sensor response was defined as the ratio between the electrical resistance in the presence of ozone and the baseline resistance (absence of O_3). The response time was defined as the time the sensor needs to reach 90% of its final electric resistance after ozone exposure, whereas recovery time was specified as the time the sensor takes to return to a resistance 10% above the one before exposure. Current-voltage (I-V) curves of the films were obtained using the same interdigitated electrodes used for gas sensing. By considering the number of trails in the electrodes, discarding film porosity and measuring the thickness, it was possible to calculate the film resistance in an applied voltage between −2 and 2 Volts. Each trail was considered an ohmic resistor.

3. Results and discussion

3.1. Microstructural analysis

To understand the influence of growth conditions, the films were deposited using powers between 15 and 240 W, which results in films of thicknesses between 96 and 190 nm depending on the film porosity. Regardless of the deposition power, the GIXRD patterns of zinc films obtained by sputtering of a metallic target agree with the zinc hexagonal structure (data not shown). After thermally treating the metallic films, the GIXRD patterns reveal a full oxidation of Zn into the ZnO crystalline wurtzite phase (gray curve in Fig. 1). As expected, the diffraction patterns of films obtained from the ceramic target show the presence of ZnO phase with a preferential growth in the (002) direction (red curve in Fig. 1). The small shift in the peak position can be related to residual stress.

Sensors were chemically characterized by XPS before gas-sensing measurements (Fig. 2). The survey spectra of films before and after thermal oxidation show no contaminants on ceramic samples and confirm the metallic and oxidized nature of zinc Zn^{2+}.

The sample surface morphology regarding the deposition conditions is evaluated by top and cross-section SEM images. Samples obtained by sputtering of the metallic target followed by thermal oxidation exhibit distinctively porous morphologies, regardless of the deposition power and with meaningful differences in their structure size (Fig. 3). It is also noticeable that higher deposition powers create bigger features and greater film thicknesses. We have opted to use the term ‘feature size’ rather than ‘grain size’ or ‘particle size’, since these structures are not formed by a single grain or particle. Although this term is not a strict definition in Materials Science, it reflects the behavior observed in our

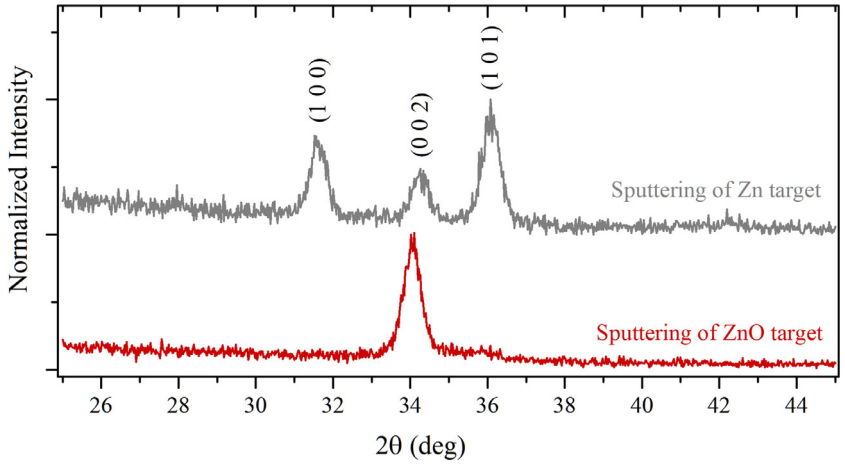

Fig. 1. Grazing-incidence x-ray diffraction patterns of films deposited on silica by sputtering both zinc metallic target after subsequent thermal oxidation (gray curve) and ZnO ceramic target (red). (For interpretation of the references to color in this figure legend, the reader is referred to the web version of this article.) .

sets of samples. Therefore, we are consciously avoiding the terms 'grain', 'crystallite' and 'particle' in this study.

The sputtering process consists in the removal of cathode's material (target) by the bombardment of energetic ions. When ejected from the target, the atoms accumulate on the substrate forming a film which final morphology is highly dependent on the energy of the arrival material and substrate temperature. As the deposition power is changed, parameters as the deposition rate and sputtered atom velocity are adjusted. The higher the power deposition, the higher the concentration of ionized argon atoms, and most importantly, higher the kinetic energy of the ions impinging the target surface. Thus, when ions velocity is high (high power), the number of atoms ejected from the target per each incident atom increase, allowing the removal of atoms clusters instead of individual ones [21]. When the atomic clusters reach the substrate, that is maintained at room temperature, they lose the energy necessary for surface diffusion and organization forming porous structures with sizes proportional to the deposition power. Contrary, when low deposition powers are used, the deposition rates are low enough (see top axis in Fig. 4) to enable the formation of compact (less porous) structures from small clusters and/or atoms.

In Fig. 4 it is possible to observe how the mean feature size changes as a function of power, and consequently of deposition rate. The feature size changes between 29 nm (for 15 W) and 124 nm (240 W), changing rapidly for powers below 60 W. Notice that the standard deviation increases with structure size. Even though the amount of material deposited is kept constant (using the quartz crystal microbalance), higher deposition powers induce the formation of more porous films. Therefore, the film thickness is not the same for all the deposition powers used.

On the other hand, films obtained from the ceramic target are completely different. Besides the preferential growth, there is another critical difference between films obtained from the ZnO target and the ones obtained from the metal Zn target. As shown in Fig. 5, these films exhibit a greatly compact morphology that highly contrasts with the porous films of Fig. 3. As observed in other studies, sputtering a ceramic target always produces compact films as a result of low deposition rates [22,23]. This compact arrange of zinc oxide columnar growth has also been observed for reactive sputtering of metallic zinc targets when the formation of zinc oxide occurs during the deposition process [24]. The top view images of films presented in Fig. 5, also show the tightly organized structures, similar to the porous films registered by Laurenti et al. [25].

From the gas-sensing perspective, this type of structures and organized films could present minor benefits. Our hypothesis is that the interaction of these films with the gaseous phase is limited to the geometric surface, which produces low and limited gas sensibility compared with that of porous films.

3.2. Gas-sensing response to ozone

The detection of ozone by ZnO films occurs as a result of oxygen adsorption at the material surface. In order to adsorb, the oxygen atom captures electrons from the conduction band, leaving a positive electron hole and forming an electron-depleted surface region [3]. In ZnO, this phenomenon is registered by increases in the electrical resistance of the film.

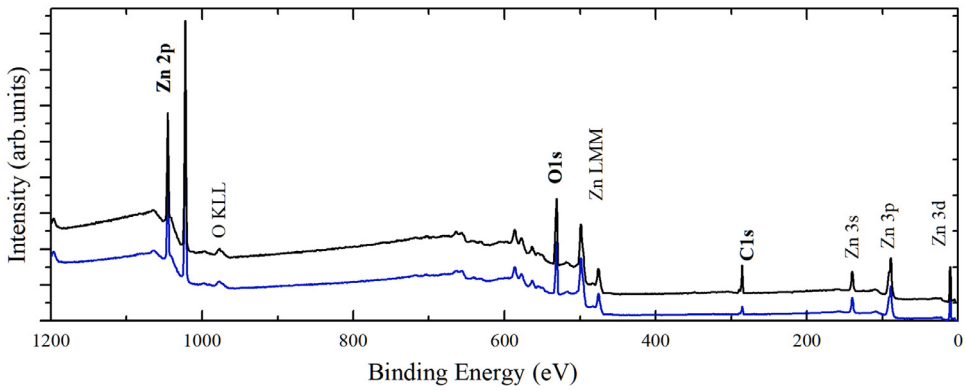

Fig. 2. XPS spectra for ZnO films obtained from the thermal oxidation of zinc film (blue curve) and sputtered directly from a ceramic target (black curve). (For interpretation of the references to color in this figure legend, the reader is referred to the web version of this article.).

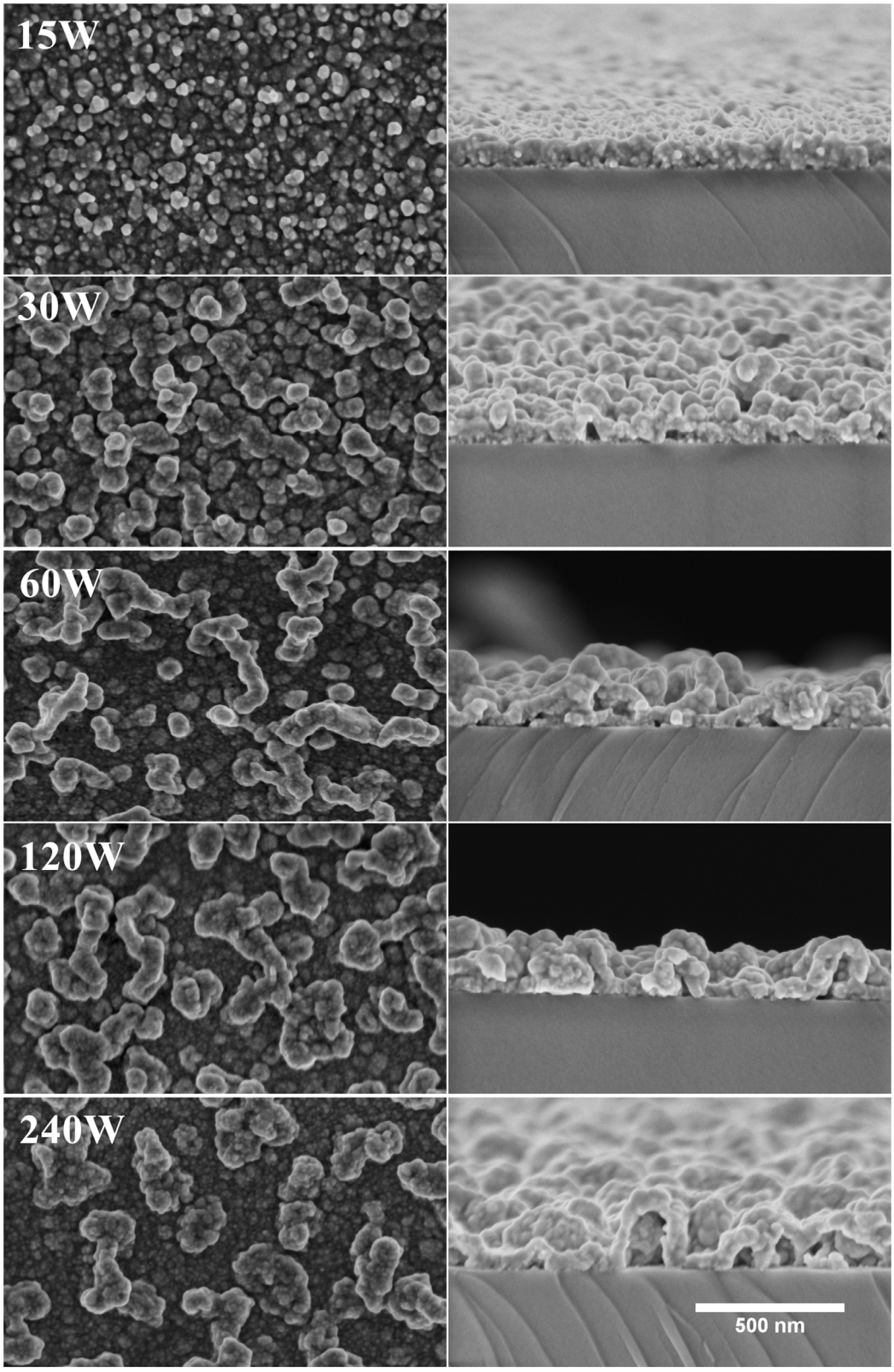

Fig. 3. Top view (left) and cross-section (right) scanning electron microscopy images of films formed by sputtering of a metallic target and subsequent oxidation. .

To find the optimum working temperature of our sensors, it was necessary to verify the film response to 0.13 ppm of ozone at 200, 250, 300 and 350 ºC. Regardless of the deposition power, all the sensors demonstrated to have a maximum response at temperatures near 300 ºC, which in turn rapidly decreases at higher temperatures. Therefore, all the subsequent measurements were made at this optimal temperature.

Firstly, we will discuss the response of sensors obtained by sputtering of metallic target,as a function of morphological differences; then, we will compare these results with the contrasting compact

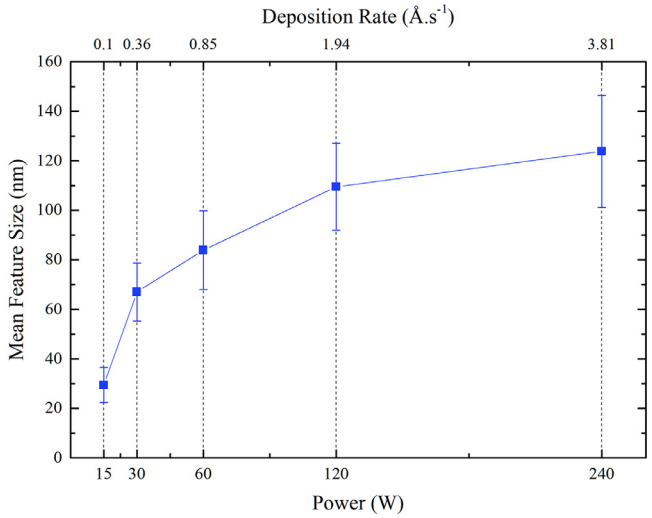

Fig. 4. Evolution of mean feature size as a function of deposition power in samples from the sputtering metallic target.

morphology of sensors produced from the ceramic target.

- *Sensors obtained by sputtering of a metallic target and thermal oxidation*.

The response of the sensors to 0.13 ppm of ozone during 30 s is shown in Fig. 6a. The electric response of all the sensors behaves as expected for n-type semiconductors in presence of oxidizing gasses, that is, there is an increase in electrical resistance. The magnitude of the response is strongly dependent on power and deposition rates, which can be explained considering the morphology and structure size of these films.

From the models used in gas sensing, it is expected that films with a larger surface area exhibit greater response. In terms of structure mean size and film porosity, it is possible to assume that smaller structures and porous films would have a bigger surface-to-volume ratio, and consequently would have greater response. In our experiments (Fig. 6b), the response to ozone is maximized for films with feature size near 84 nm (deposited with 60 W), which in turn rapidly decreases for bigger or smaller structures.

From top and cross-section SEM images in Fig. 3, it can be concluded that films with the smallest feature sizes (15 W and 30 W) present more compact structures. Low deposition rates inhibit the formation of porous structures, which can limit the material interaction with the gaseous phase and restrict the gas sensor response, as also reported by Colmenares et al. [18]. On the other hand, the opposite is observed in films deposited with higher powers, where the deposition rates allow bigger structures to reach the substrate in such a rapid way that surface diffusion is not possible and the formation of cavities and "chambers" between particles aggregates is promoted

Althougth it is not possible to performe a direct measurement of the film's porosity, we can do an estimation of the apparent porosity if we remember the amount of material deposited is fixed to be always the same so differences in thicknesses is determined by the final thickness of the porous film. Fig. 7 show the apparent porosity of the films, calculated from $\varnothing = 1 + h_{deposit}/h_{porous}$, as funtion of the power of deposition.

The results of morphology and gas sensing suggest that the surface area available for gas adsorption is a compromise between structure size and film porosity. Even though a small feature size implies a bigger surface-to-volume ratio, the film porosity is so low that the surface available for adsorption is small. On the other extreme, although higher deposition rates produce highly porous films, very large structures can reduce the surface-to-volume ratio, also diminishing the surface area for adsorption. In our experiments, the sensor that reunites the best combination of porosity and feature size is the film deposited with 60 W (feature size of 84 nm).

We must consider the possibility that ZnO films with different concentration of charge carriers could potentially affect the ZnO conductivity and explain the difference in the sensor response. Even though the deposition method and thermal treatment were the same for all the samples, different deposition powers could have produced zinc oxide films with differences in the electronic band structure or defect density. Therefore, to avoid misconclusions and affirm that ZnO different responses are caused by apparent differences in the surface area, it was necessary to investigate the electrical properties of ZnO films.

I-V curves of ZnO films were measured in order to determine film resistivity. As shown at the inset of Fig. 8, all I-V curves confirm the ohmic contact between the film and the electrode, which allows us to discard the possible influence regarding the type of contact on the electrical measurements.

The resistivity values found for ZnO films range between 10^3 and 10^6 Ω cm, which are consistent with those reported for ZnO sputtered films. These high values are usually associated with the absence of defects responsible for the conductivity of the ZnO matrix (oxygen vacancies) [26,27]. As exhibited in Fig. 8, the film with the biggest resistivity of 1 MΩ cm is the one deposited with 60 W (biggest gas response), while small deposition powers generate films with the smallest resistivity values.

According to *Lu and Wong* [27] the thermal treatment conditions (atmosphere, temperature and time) are the ones that most influence the ZnO resistivity. In our case, as the thermal treatment to obtain ZnO films is the same for all the powers, we can deduce that the population of ZnO defects is approximately the same for all the samples, and the differences in resistivity come from the structure size and porosity. The lowest resistivity can be directly associated with the most compact film (film deposited with 15 W), where the current easily goes through. On the other hand, when the deposition power is increased, the film volume occupied by pores also increases, limiting the current flux and causing an increment in resistivity until reaching a maximum value of approximately 1 MΩ cm. For films deposited with 120 and 240 W, an opposite tendency is observed, that is, the film resistivity starts decreasing until reaching 58% of its maximum value. Despite the increase

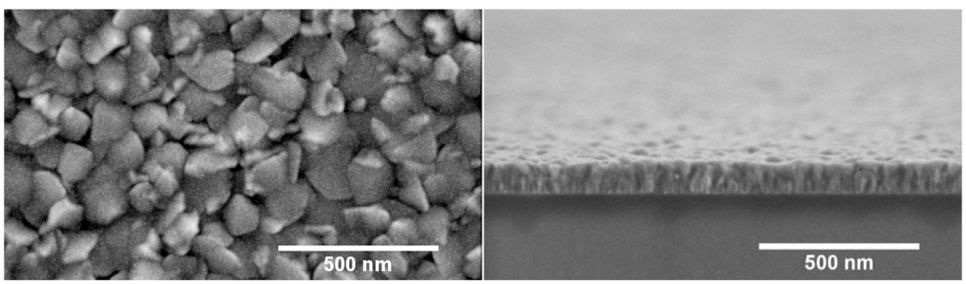

Fig. 5. Top and cross-section SEM images of ZnO films formed by sputtering of a ceramic target. The films obtained this way are more compact than the ones obtained by sputtering of a metallic target.

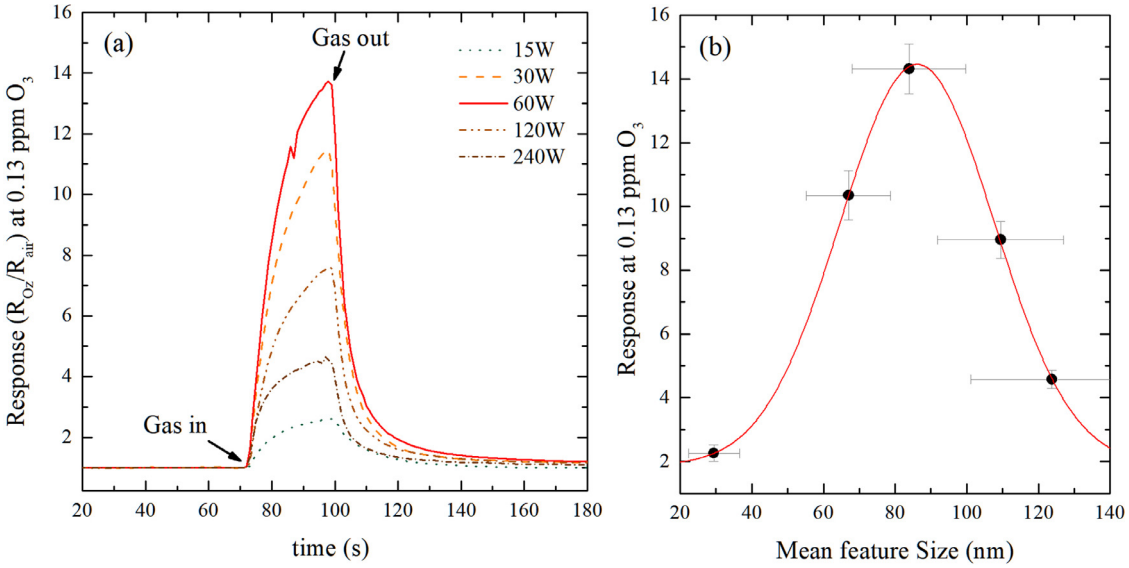

Fig. 6. Ozone gas-sensing response of ZnO films deposited by sputtering of a metallic target and synthetized with different powers. The response is obtained by exposing at 0.13 ppm of ozone at 300 °C working temperature (a). Response to ozone vs. mean feature size and gaussian fit of experimental points (b). The mean feature size of sensors was estimated using the top view SEM images of Fig. 3.

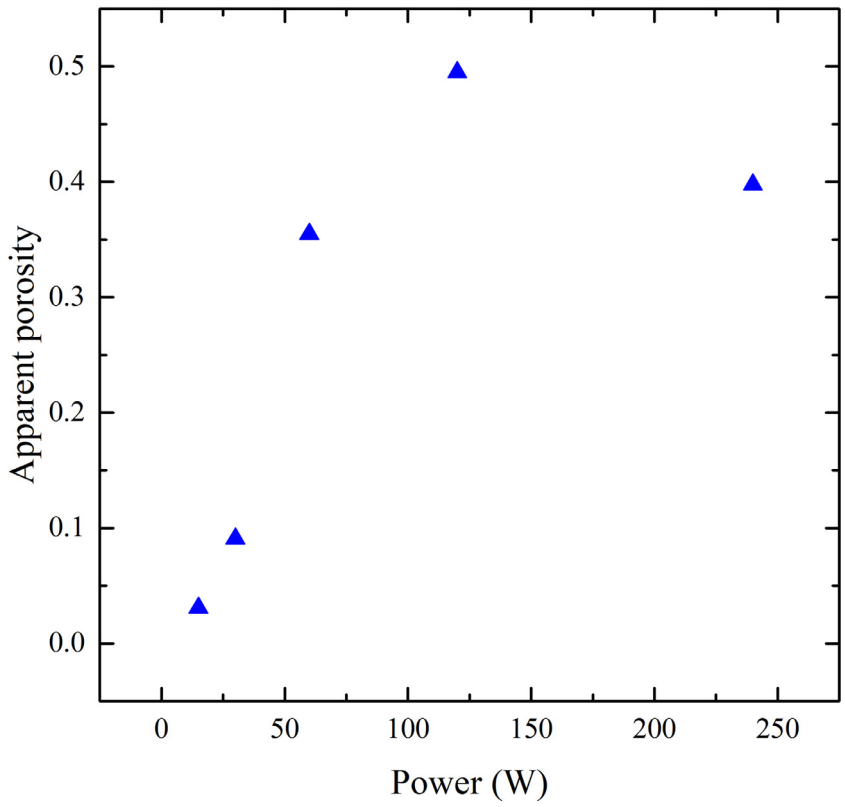

Fig. 7. Apparent porosity of ZnO films deposited with different powers by sputtering of metallic target. The apparent porosity is estimated by the amount of material deposited and the final thickness driven by the porosity of the film.

in the pore volume, there is another factor that must be considered: big features facilitate the electron current flow more than the feature size of a 60 W sensor with smaller structures.

To confirm the absence of differences in composition and electronic structures of sputtered samples, we use band-gap energy. Fig. 9 shows the absorbance spectra and the Tauc plot used to calculate the band-gap energy. All film band gaps result in values around 3.20 eV with irrelevant variations between samples. These results confirm that sputtering deposition power does not affect band-gap energy [28].

Since our sensors are chemically indistinguishable, the differences in the response magnitude may be completely attributed to the morphologic differences and the amount of surface area that each sensor has available for gas interaction.

- Gas *Sensor obtained by sputtering of a ceramic target.*

Films deposited from a ZnO ceramic target and deposition power of 240 W showed to have the lowest electrical response to ozone

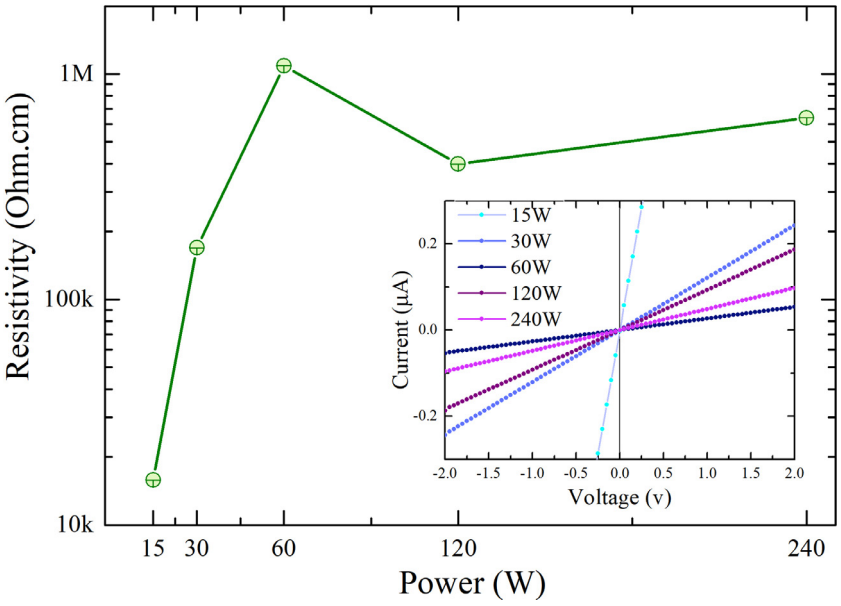

Fig. 8. Resistivity of ZnO films as a function of deposition power; at the inset, the I-V curves were used to obtain the resistivity.

(0.13 ppm) among the ZnO sensors studied in this work. The response (R_{ozone}/R_{air}) = 1.7 is less than half of the one showed for the sensor deposited from a metallic target with deposition power of 15 W. According to the conclusions established in the previous section, we can suppose that the compact morphologies and faceted surfaces of films deposited from ceramic targets restrict the area available for O_3 adsorption. Their dense morphology and preferential growth also affect film resistivity. Data of current vs. potential measurements (curves not shown) reveal a characteristic ohmic contact and film resistivity from the order of 10^2 Ω cm.

Table 1
Response and recovery times of sensors obtained by sputtering of ceramic and metallic targets followed by thermal evaporation.

Target	Sample	Response time (s)	Recovery time (s)
Metallic target	ZnO _ 15 W	30	26
	ZnO _ 30 W	30	29
	ZnO _ 60 W	42	29
	ZnO _ 120 W	39	36
	ZnO _ 240 W	26	42
ZnO	ZnO _ 240 W	181	178

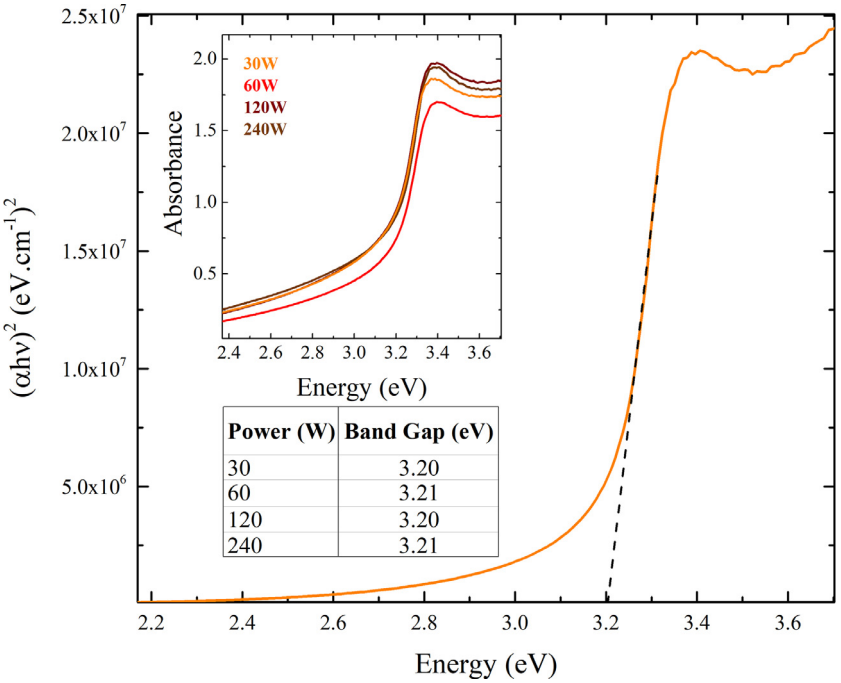

Fig. 9. Absorbance spectra of zinc oxide films deposited with different deposition powers (inset) and Tauc plot to calculate band-gap values from the intercept with the energy axis.

3.3. Response and recovery times

Response and recovery times were determined by exposing all the sensors to 0.13 ppm of ozone until the sample resistance reached an equilibrium value at 300 ºC (Table 1).

All the sensors produced from the metallic target presented characteristic times below 42 s. Considering that they are chemically indistinguishable, as stated before, the density of surface adsorption centers would be the same for any power, and the differences in adsorption site numbers are caused by the distinct surface area. Therefore, sensors with greater surface area take more time to occupy all the adsorption centers, and consequently have higher response times (sensor deposited with 60 W). On the other hand, the low-porosity sensor deposited with the lowest power (15 W) has the lowest response time, reaching 90% of its total response after 25 s of exposure. The same response time of 25 s is measured for the sensor deposited with 240 W, which despite having great porosity, has the greatest structure sizes that are responsible for decreasing its surface area.

The response and recovery times of the sensor obtained from the ceramic target are considerably greater than those observed for porous films. In spite of the low surface area available for adsorption, high response times presented by these sensors raise the possibility of gas detection by another process other than adsorption of oxygen at the sample surface. As exposed in other works, there is a possibility of film-gas interaction through gas diffusion process [4,29,30], which would involve longer times and higher temperatures to make it possible.

3.4. Response curve of ZnO–60 W with increasing gas concentrations

As the zinc oxide sensor deposited from a metallic target and with a power of 60 W exhibits the highest response, its performance in increasing ozone concentrations is studied. As shown in Fig. 10, the resistance change at different ozone concentrations varies proportionally to gas concentration.

The lack of a saturation point indicates that the sensor detection limits are likely higher than the values studied here. After exposing the sensor to the greatest concentration of target gas (0.89 ppm), another exposure to 0.13 ppm of ozone is performed. The electrical resistance is in good agreement with the value observed in the first cycle, which confirms the total recovery of the sensor to its original state and discards the possibility of film degradation or irreversible reactions during the detection process.

The response of the sensors to hydrogen was also investigated. A typical dynamic-response curve is shown in Fig. 11. It is important to notice that the response of these ZnO thin films towards reducing gasses is much lower than the typical response to oxidizing gasses which suggests that the films fabricated using the proposed methodology exhibit good selectivity.

Regarding the stability of the sensor properties in relation to time, the response of this sensor (deposited using 60 W) is studied after several days of film production. The measurements between 0 and 100 days after film production (by sputtering and subsequent oxidation) exhibit a response variation around 5%, which depicts the chemical stability of ZnO films.

4. Conclusions

This work presents the gas-sensing performance of zinc oxide thin films deposited with different growth conditions and from distinct target materials. The morphology is studied in order to understand how differently films react to the presence of ozone.

The target type used to produce ZnO films influences the final morphology of the film structures and the magnitude of their response to ozone. Ceramic targets produce compact and organized structures, while metallic targets create films with low density and great porosity. Whereas the response of the sensor produced from the ceramic target is limited up to 1.7 at 0.13 ppm of O_3, the porous film produced by sputtering of the metallic target followed by thermal oxidation can reach responses up to 14 for 0.13 ppm of ozone and 1.2 for 242 ppm of hydrogen.

Moreover, the deposition power also controls the dynamics of the sputtering process, having a great effect on the size and porosity of zinc oxide films deposited from a metallic target. The films have structure sizes and porosities proportional to the deposition power, which enables us to use the energy of the argon atoms (controlled by the deposition power) as a tuning factor for desirable morphologies. Lower deposition powers tend to create smaller and compact structures with low response and fast response time, while higher deposition powers create bigger structures with low response and slow response time. In our system, it was possible to achieve the best condition of porosity and structure size, responsible for maximizing the sensor response (circa 14 at 0.13 ppm of O_3) in films deposited with 60 W.

CRediT authorship contribution statement

Y.N. Colmenares: Conceptualization, Methodology, Investigation, Formal analysis, Writing - original draft, Writing - review & editing. **W. Correr:** Methodology, Formal analysis, Validation, Writing - original

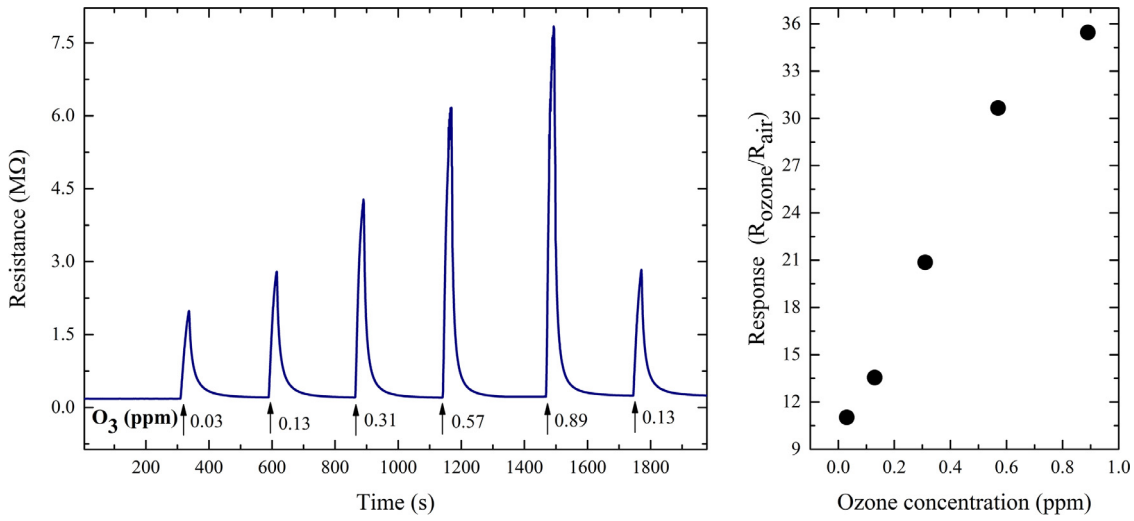

Fig. 10. (Left) Electrical resistance of the ZnO sensor deposited from a metallic target and with a power of 60 W. The sensor is exposed to different ozone gas concentrations during 30 s with intervals of 5 min. (Right) Sensor response as a function of ozone concentration.

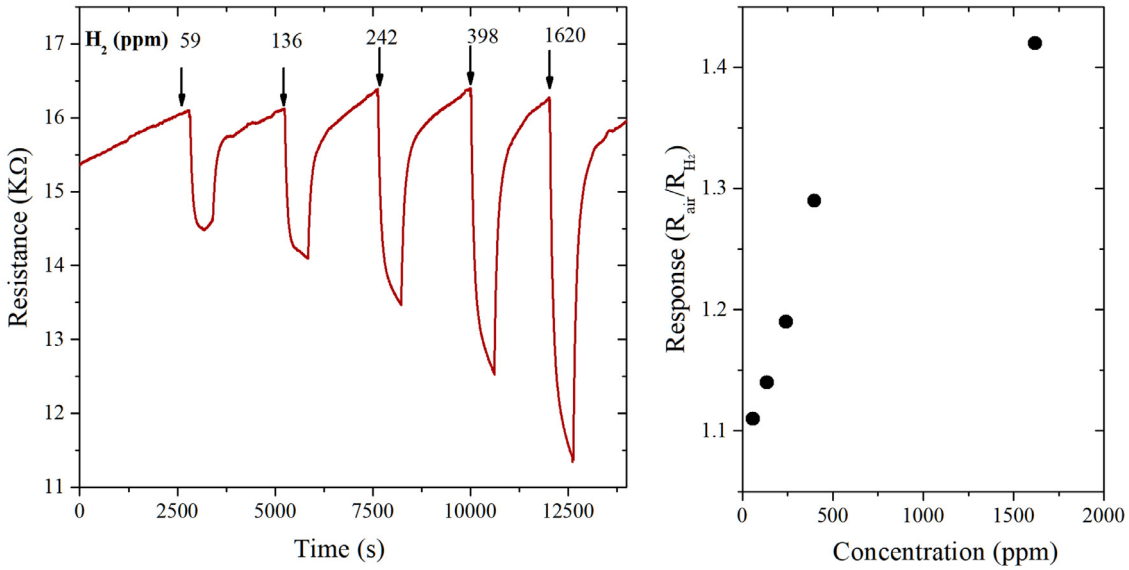

Fig. 11. (Left) Electrical resistance of the ZnO sensor deposited from a metallic target and with a power of 60 W. The sensor is exposed to different hydrogen gas concentrations during 10 min with intervals of 30 min. (Right) Sensor response as function of hydrogen concentration.

draft. **B.S. Lima:** Formal analysis, Writing - review & editing, Visualization. **V.R. Mastelaro:** Conceptualization, Supervision, Validation, Funding acquisition.

Declaration of Competing Interest

The authors declare that they have no known competing financial interests or personal relationships that could have appeared to influence the work reported in this paper.

Acknowledgments

This work has been supported by the Brazilian research financing institutions FAPESP/CEPID (grant nos. 2013/09573-3, 2013/07296-2, 2015/20124-1, and 2012/15170-6) and CNPq. The authors would like to thank the Microfabrication Laboratory at the Brazilian Nanotechnology National Laboratory (LNNano), Campinas, SP, Brazil (Project LMF-18580); the Electronic Microscopy Laboratory from the Research Support Center in Advance Materials (NAP-MA-USP), São Paulo, SP, Brazil; and the Laboratory of Electron Microscopy from the Technology Center for Hybrid Materials (CTMH), São Carlos, SP, Brazil.

References

[1] E. Comini, Metal oxide nanowire chemical sensors: innovation and quality of life, Mater. Today. 19 (2016) 559–567, https://doi.org/10.1016/j.mattod.2016.05.016.
[2] M. Batzill, Surface science studies of gas sensing materials: SnO_2, Sensors 6 (2006) 1345–1366, https://doi.org/10.3390/s6101345.
[3] C. Wang, L. Yin, L. Zhang, D. Xiang, R. Gao, Metal oxide gas sensors: sensitivity and influencing factors, MDPI Sensors (2010) 2088–2106, https://doi.org/10.3390/s100302088.
[4] N. Barsan, D. Koziej, U. Weimar, Metal oxide-based gas sensor research : how to ? Sensors Actuators B Chem. 121 (2007) 18–35, https://doi.org/10.1016/j.snb.2006.09.047.
[5] L. Liu, L. Shouchun, Z. Juan, W. Lianyuan, Z. Jinbao, L. Haiying, L. Zhen, H. Yu, J. Xiaoxue, Z. Peng, Improve selective acetone sensing properties of Co-doped ZnO nanofibers by electrospining, Sensors Actuators B. Chem. (2011) 782–788, https://doi.org/10.1016/j.snb.2011.01.047.
[6] M.H. Darvishnejad, A. Anaraki Firooz, J. Beheshtian, A.A. Khodadadi, M. Moliner, C. Martínez, A. Corma, M.E. Davis, E. Hu, Z. Lai, K. Wang, J.P. Zhai, W.W. Peng, I.N. Li, S.C. Ruan, Z.K. Tang, Y. Ma, N. Li, S. Xiang, N. Guan, B. Han, C.H. Shin, P.A. Cox, S.B. Hong, W. Yan, E.W. Hagaman, S. Dai, J. Weitkamp, P. Luthar, C. Martin, N. Tosi-Pellenq, J. Patarin, J.P. Coulomb, Highly sensitive and selective ethanol and acetone gas sensors by adding some dopants (Mn, Fe, Co, Ni) on hexagonal ZnO plates. J. Phys. Chem. C. 26 (2014) 7838–7845, https://doi.org/10.1039/C5RA24169C.
[7] W. Belkacem, A. Labidi, J. Gu, N. Mliki, K. Aguir, Cobalt nanograins effect on the ozone detection by WO 3 sensors, Sensors Actuators B. Chem. 132 (2008) 196–201, https://doi.org/10.1016/j.snb.2008.01.023.
[8] H.-J. Kim, J.-H. Lee, Highly sensitive and selective gas sensors using p-type oxide semiconductors: overview, Sensors Actuators B Chem. 192 (2014) 607–627, https://doi.org/10.1016/j.snb.2013.11.005.
[9] C.S. Moon, H.R. Kim, G. Auchterlonie, J. Drennan, J.H. Lee, Highly sensitive and fast responding Co sensor using SnO_2 nanosheets, Sensors Actuators, B Chem. 131 (2008) 556–564, https://doi.org/10.1016/j.snb.2007.12.040.
[10] M.R. Alenezi, S.J. Henley, N.G. Emerson, S.R.P. Silva, From 1D and 2D ZnO nanostructures to 3D hierarchical structures with enhanced gas sensing properties, Nanoscale 6 (2014) 235–247, https://doi.org/10.1039/C3NR04519F.
[11] L.F. Da Silva, A.C. Catto, W. Avansi, L.S. Cavalcante, V.R. Mastelaro, J. Andr??s, K. Aguir, E. Longo, Acetone gas sensor based on alpha-Ag2WO4 nanorods obtained via a microwave-assisted hydrothermal route, J. Alloys Compd. 683 (2016) 186–190, https://doi.org/10.1016/j.jallcom.2016.05.078.
[12] C. Shao, Y. Chang, Y. Long, High performance of nanostructured ZnO film gas sensor at room temperature, Sensors Actuators, B Chem. 204 (2014) 666–672, https://doi.org/10.1016/j.snb.2014.08.003.
[13] Dian-Xing Ju, H.-Y. Xu, Z.-W. Qiu, Z.-C. Zhang, Q. Xu, J. Zhang, J.-Q. Wang, B.-Q. Cao, Near room temperature, fast-response, and highly sensitive triethylamine sensor assembled with au-loaded ZnO/SnO_2 core-shell nanorods on flat alumina substrates, Appl. Mater. Interfaces. 7 (2015) 19163–19171, https://doi.org/10.1021/acsami.5b04904.
[14] J. Zhang, X. Liu, S. Wu, B. Cao, S. Zheng, One-pot synthesis of Au-supported ZnO nanoplates with enhanced gas sensor performance, Sensors Actuators B. Chem. 169 (2012) 61–66, https://doi.org/10.1016/j.snb.2012.02.070.
[15] N. Barsan, U. Weimar, Conduction model of metal oxide gas sensors, J. Electroceramics. 7 (2001) 143–167, https://doi.org/10.1023/A:1014405811371.
[16] L. Zhu, W. Zeng, Physical room-temperature gas sensing of ZnO-based gas sensor : a review, Sensors Actuators A. Phys. 267 (2017) 242–261, https://doi.org/10.1016/j.sna.2017.10.021.
[17] S. Ji, C. Ye, Synthesis, growth mechanism, and applications of zinc oxide nanomaterials, J. Mater. Sci. Technol. 24 (2008) 457–472.
[18] N. Colmenares, W. Correr, V.R. Mastelaro, Deposition rate influence in O3 sensing response of sputtered ZnO thin films, in: Proc. Eurosensors 2017, Paris - France, 2017. doi:10.3390/proceedings1040429.
[19] M. Bender, E. Gagaoudakis, E. Douloufakis, E. Natsakou, N. Katsarakis, V. Cimalla, G. Kiriakidis, E. Fortunato, P. Nunes, A. Marques, R. Martins, Production and characterization of zinc oxide thin films for room temperature ozone sensing, Thin Solid Films 418 (2002) 45–50, https://doi.org/10.1016/S0040-6090(02)00588-6.
[20] M. Bender, E. Fortunato, P. Nunes, I. Ferreira, A. Marques, R. Martins, N. Katsarakis, V. Cimalla, G. Kiriakidis, Highly sensitive ZnO ozone detectors at room temperature, Jpn. J. Appl. Physics, Part 1 Regul. Pap. Short Notes Rev. Pap. 42 (2003) 10.11432Fjjap.42.l435.
[21] M. Ohring, Materials Science of Thin Films, 2nd Edition, (2001), https://doi.org/10.1016/B978-0-12-524975-1.50018-5 Boston.
[22] G.N. Jackson, R.F. Sputtering, Thin Solid Films 5 (1970) 209–246.
[23] L.P. Schuler, M.M. Alkaisi, P. Miller, R.J. Reeves, A. Markwitz, Comparison of DC and RF sputtered zinc oxide films with post-annealing and dry etching and effect on crystal composition, Jpn. J. Appl. Physics, Part 1 Regul. Pap. Short Notes Rev. Pap. 44 (2005) 7555–7560, https://doi.org/10.1143/JJAP.44.7555.
[24] R. Nandi, S.S. Major, The mechanism of growth of ZnO nanorods by reactive sputtering, Appl. Surf. Sci. 399 (2017) 305–312, https://doi.org/10.1016/j.apsusc.2016.12.097.

[25] M. Laurenti, G. Canavese, S. Stassi, M. Fontana, M. Castellino, C.F. Pirri, V. Cauda, A porous nanobranched structure: an effective way to improve piezoelectricity in sputtered ZnO thin, RSC Adv. 6 (2016) 76996–77004, https://doi.org/10.1039/c6ra17319e.

[26] D.L. Raimondi, E. Kay, High resistivity transparent ZnO thin films, J. Vac. Sci. Technol. A Vacuum, Surfaces, Film. 7 (1970), https://doi.org/10.1116/1.1315841.

[27] L. Lu, M. Wong, S. Member, The resistivity of zinc oxide under different annealing configurations and its impact on the leakage characteristics of zinc oxide thin-film transistors, IEEE Trans. Electron Devices. 61 (2014) 1077–1084, https://doi.org/10.1109/TED.2014.2302431.

[28] A. Ismail, M.J. Abdullah, The structural and optical properties of ZnO thin films prepared at different RF sputtering power, J. King Saud Univ.–Sci. 25 (2013) 209–215, https://doi.org/10.1016/j.jksus.2012.12.004.

[29] J. Zhang, S. Wang, M. Xu, Y. Wang, B. Zhu, S. Zhang, W. Huang, S. Wu, Hierarchically porous ZnO architectures for gas sensor application, Cryst. Growth Des. 9 (2009) 3532–3537, https://doi.org/10.1021/cg900269a.

[30] J. Zhu, O.K. Tan, Y.C. Lee, T.S. Zhang, B.Y. Tay, J. Ma, Hierarchical porous/hollow tin oxide nanostructures mediated by polypeptide: surface modification, characterization, formation mechanism and gas-sensing properties, Nanotechnology 17 (2006) 5960–5969, https://doi.org/10.1088/0957-4484/17/24/010.